

# ROTOR MECHANICAL STRESS ANALYSIS OF A DOUBLE-SIDED AXIAL FLUX PERMANENT MAGNET MACHINE

## MEHANSKA ANALIZA ROTORJEV DVOSTRANSKEGA SINHRONSKEGA STROJA Z AKSIJALNIM MAGNETNIM PRETOKOM

Franjo Pranjič<sup>31</sup>, Peter Vrtič<sup>1</sup>

**Keywords:** Axial flux permanent magnet machine (AFPMM), mechanical stress analysis (MSA), rotor thickness

### Abstract

This paper presents the mechanical stress analysis (MSA) of a rotor disk in a double-sided axial flux permanent magnet machine (AFPMM). The analysis considers the rotor of a prototype AFPMM with a double external rotor and single internal stator. Rotor disks of the prototype AFPMM are constructed of two 11.6 mm-thick steel disks and represent around 50% of the total weight of the machine. The new rotor disk thickness was determined based on a rotor axial displacement due to the attractive force between the permanent magnets on opposite rotor disks.

### Povzetek

Članek predstavlja mehansko analizo rotorjev dvostranskega sinhronskega stroja s trajnimi magneti in aksijalnim magnetnim pretokom. Analiziran je rotor prototipa stroja, ki ima dvojni zunanji rotor ter notranji stator. Rotor analiziranega stroja je izdelan iz dveh 11,6 mm debelih

---

<sup>31</sup> Corresponding author: Franjo Pranjič, Tel.: +386 3 777402, Mailing address: Koroška cesta 62a, E-mail address: [franjo.pranjic@um.si](mailto:franjo.pranjic@um.si)

<sup>1</sup> University of Maribor, Faculty of Energy Technology, Hočevarjev trg 1, 8270 Krško

jeklenih diskov, kar predstavlja približno 50% skupne teže stroja. Trajni magneti na nasproti ležecih rotorskih diskih povzročajo pritezne sile med rotorskimi diski, ki se posledično upognejo. Na podlagi upogiba rotorskih diskov pa je določena nova debelina le-teh.

## 1 INTRODUCTION

Axial flux permanent magnet machines have been becoming increasingly popular lately due to their compactness, high degree of reliability, efficiency, simple construction and high-power density, [2-6]. This type of machine is also called “a disk-type machine” and has various topologies:

- Single-sided (one stator and one rotor)
- Double-sided (single stator-double rotor or single rotor-double stator)
- Multistage (multiple rotors and stators).

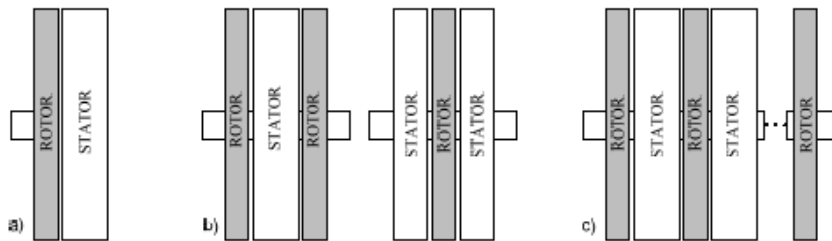


**Figure 1:** Basic topologies of AFPMM: a) single-sided, b) double-sided, c) multistage

All the above-mentioned topologies can be constructed with or without iron cores (coreless) and with surface-mounted or buried permanent magnets (PMs). Low power permanent magnet machines are usually constructed with coreless stators and steel rotors with surface mounted PMs, [1].

Each machine topology has its own strengths and weaknesses. Topologies without stator cores are used for low- and medium-power generators and have various advantages, including the absence of cogging torque, as well as their linear torque-current characteristics, high power density, and compact construction. Due to the absence of the core losses, these types of generators can operate with a higher efficiency compared to the conventional generators, [7].

Mechanical stress analysis (MSA) has been presented in several publications. In [9], the authors present the MSA for a high-speed AFPMM and analyse the stress level of the rotor disks due to the high-speed rotation, using the three-dimensional finite element method (3D FEM). Fei et al. present the simplified 2D and 3D FEM for analysis and design of rotor disks of high-speed AFPM generators in [10]. Rani et al. present the computational method of rotor stress analysis for conventional rotors using J-MAG software in [11]. In [14], the authors presented the structural analysis of low-speed axial-flux permanent-magnet machines.

Vrtic, [12], analysed the rotor disk thickness of the same prototype AFPMM concerning the magnetic flux density magnitudes.

This article firstly presents the double-sided AFPMM with an internal coreless stator and two external rotors and its characteristics, with a focus on the selected dimensions of rotor disks. The

prototype AFPMM was analytically analysed in [7] and optimized in [8] by using evolutionary optimization with a genetic algorithm and an analytical evaluation of objective functions. Since the thickness of the rotor disks was not included in the optimization (due to the assumed infinite permeability), this article presents the mechanical stress analysis (MSA) of the rotor disks used in the prototype machine and, based on the results, a new rotor disk thickness is determined.

The mechanical stress analysis in this article is accomplished by:

1. analytically calculating the pressure caused by the PMs on opposite disks and the attractive force between them,
2. simulating the stress distribution and deflection of the disks with Solidworks software based on the calculated magnetic pressure and force,

The primary reason for the rotor optimization lies in the fact that the weight of the two rotor disks represents about 50% of the total weight of the machine, [1].

## 2 AFPMM PROTOTYPE

The AFPMM considered in this article is a double-sided AFPMM with two external rotors and one internal coreless stator. Figure 2 shows the geometric parameters, and Table 1 shows the optimized data of the analysed prototype AFPMM.

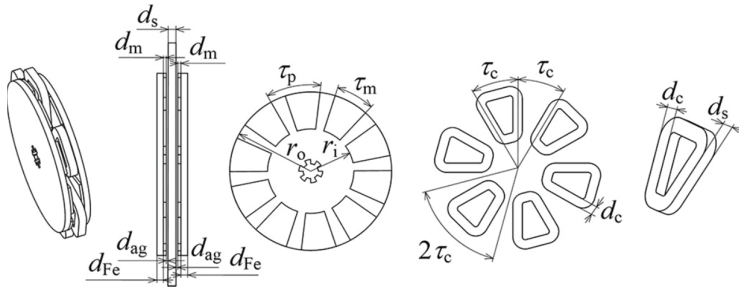


**Figure 2, [8]:** Geometric parameters of the AFPMM

The PMs used in the prototype AFPMM are neodymium magnets (NdFeB). Figure 3 shows the PMs; their characteristics are presented in Table 2, where:

- $B_r$  is the remanent magnetic flux density,
- $H_{cB}$  is the coercive magnetic field intensity of the magnetic flux density,
- $H_{cJ}$  is the coercive magnetic field intensity of the polarization,
- $(BH)_{max}$  is the maximum energy product, and
- $T_{max}$  is the maximum working temperature of PMs

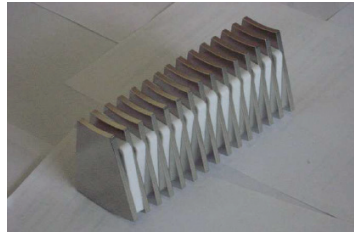


**Figure 3, [17]:NdFeB permanent magnets used in the prototype AFPMM**

**Table 1: GEOMETRY AND PARAMETERS OF ANALYSED AFPMM**

	Symbol	Quantity	Value/Unit
ROTOR	$R$	Rotor disk radius	150 mm
	$d_{Fe}$	Rotor disk thickness	11,6 mm
	$d_M$	Permanent magnet thickness	5 mm
	$\tau_m$	Magnetic pole pitch	25°
	$R_{IPM}$	Inner radius of PM	80 mm
	$R_{OPM}$	Outer radius of PM	150 mm
	$B_r$	Remanent magnetic flux density	1,22 T
	$\tau_p$	Pole pitch	36 °
	$p$	Number of pole pairs	5
	STATOR	$I$	Rated phase current
$A$		Electrical current density	5 A/mm <sup>2</sup>
$P$		Rated power at 1500 min <sup>-1</sup>	4,4 kW
$N$		Number of turns per coil	50
		Number of coils	12 (2x6)
$d_c$		Coil width	20 mm
$d_s$		Stator thickness	15 mm
$\tau_c$		Coil pitch	30°
$m$		Number of phases	3
$d_{ag}$		Air-gap thickness	1mm
$S_w$	Copper wire cross section	2,46 mm <sup>2</sup>	

**Table 2: PROPERTIES OF PERMANENT MAGNETS USED IN PROTOTYPE AFPMM**

Type of PM	$B_r$		$H_{cB}$	$H_{cJ}$	$(BH)_{max}$		$T_{max}$
	(T)	(kA/m)			(kA/m)	(kJ/m <sup>3</sup> )	
38SH	min	max	907	1592	min	max	150
	1,22	1,25			287	310	

## 2.1 Stator design

The internal stator is constructed from non-magnetic polypropylene square plate with dimensions of 400×400×15mm. Each side of the plate has a carved space for six coils, four thermocouples, and slots for the conductors (Figure 4a). After the conductors are inserted in the slots, a varnish is applied, and the stator is ready for mounting (Figure 4b).

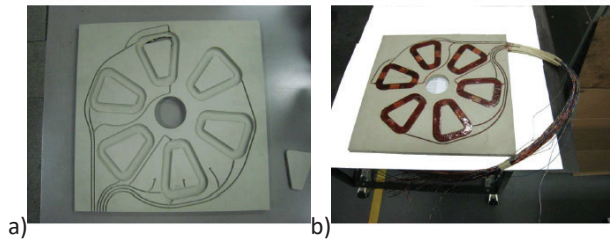


**Figure 4, [17]: a) Stator support structure, b) Stator ready for mounting**

## 2.1 Rotor design

Rotor disks are constructed from structural steel (St52), which has adequate magnetic properties and a suitable price. From the safety point of view, the thickness selected for the disks was 12 mm. After balancing, the final thickness was 11.6 mm.

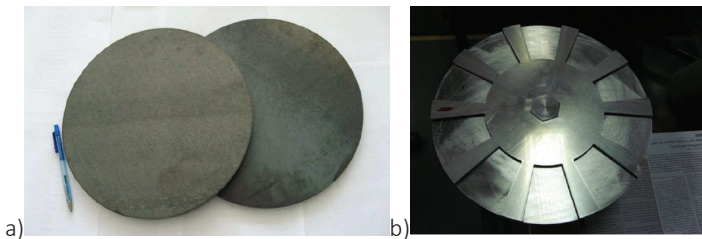


**Figure 5, [17]: a) Unbalanced rotor disks, b) Balanced rotor disk with an accessory for gluing the PMs on the rotor disk**

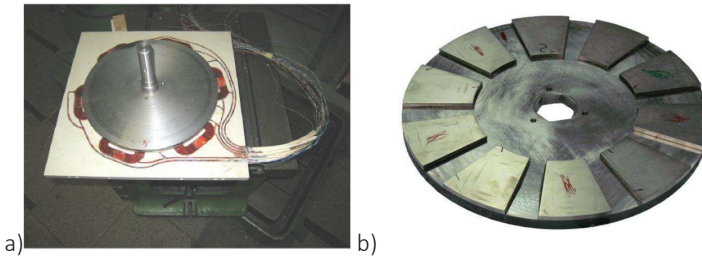


Figure 6, [7]: a) Stator and double rotor with the shaft, b) Rotor disk with PMs

### 3 METHODS AND RESULTS

The mechanical stress analysis was performed numerically and analytically, using the Solidworks simulation tool.

Solidworks software simulates the magnetic pressure of the PMs on the rotor disk and determines the stress distribution and deflection using the Finite Element method (FFEPlus, i.e. Fourier Finite Element Plus algorithm).

In finite element analysis, a problem is represented by a set of algebraic equations that must be solved simultaneously. FFEPlus is an iterative method that solves the equations using approximate techniques; a solution is assumed for each iteration, and the associated errors are evaluated. The iterations continue until the errors become acceptable, [13].

Since the attractive forces of PMs are high, the deflection of the disk must not be too high due to the safety reasons, such as preventing the PMs from crashing into stator surface, preventing distortion of the air gap and consequently the characteristics of the prototype AFPMM.

#### 3.1 Parameter selection and calculation

Maxwell stress is the link between electromagnetic and structural designs. It is represented by the magnetic attraction force acting between the rotor disks. Classical analysis of magnetic equivalent circuits can be used to determine the airgap flux density and hence the Maxwell stress is given by [14]:

$$q = \frac{B_d^2}{2\mu_0} \tag{3.1}$$

where  $B_d$  is the airgap flux density and  $\mu_0$  - permeability of free space ( $4\pi \cdot 10^{-7}$  Vs/Am) [14]. The magnetic flux density in the air gap is determined by equation (3.2) [1]:

$$B_d = \frac{B_r}{1 + (d_{ag} + 0,5d_s) \frac{\mu_{rec} k_{sat}}{d_M}} \tag{3.2}$$

$$k_{sat} = 1 + \frac{l_{Fc}}{2\mu_r (d_{ag} + 0,5d_{Fc})} \tag{3.3}$$

$$\mu_{rec} = \frac{1}{\mu_0} \frac{\Delta B}{\Delta H} \quad (3.4)$$

where  $B_d$  is the magnetic flux density in the air gap,  $B_r$  is the remenent magnetic flux density of the PM,  $d_{ag}$  is the air gap thickness,  $d_s$  is the stator thickness,  $d_{Fe}$  is the rotor disk thickness,  $d_m$  is the PM thickness,  $k_{sat}$  is the saturation factor for iron,  $\mu_r$  is the permeability of the steel,  $\mu_{rec}$  is the relative recoil permeability, which is determined with the data of the magnets in Table 2.

The attractive force between PMs on opposite disks can be calculated as magnetic pressure multiplied by the active surface area of all PMs  $S_{PM}$  as shown in [1]:

$$F = \frac{B_d^2}{2\mu_0} (S_{PM}) \quad (3.5)$$

$$S_{PM} = \alpha_i \frac{\pi}{4} (D_{out}^2 - D_{in}^2) \quad (3.6)$$

$$\alpha_i = \frac{\alpha_{PM} 2p}{360} \quad (3.7)$$

Where  $\alpha_i$  is the coefficient that is calculated with the angle of PMs multiplied by the number of PMs per rotor disk (poles) and divided by 360 degrees.

Using the previously-described equations, data needed for the simulation was determined as shown in Table 3.

**Table 3: GEOMETRY AND PARAMETERS OF ANALYSED AFPMM**

Symbol	Quantity	Value/Unit
$q$	Magnetic pressure caused by the PMs	74496 Pa
$S_{PM}$	Active area of all PMs	0,0351 m <sup>2</sup>
$F$	Attractive force between rotor disks	2615 N
$d_m$	Permanent magnet thickness	5 mm
$B_d$	Peak value of magnetic flux density in the air gap	0,4327 T
$d_{ag}$	Air-gap thickness	1mm
$d_s$	Stator thickness	15 mm
$\mu_{rec}$	Relative recoil permeability	1,0704
$k_{sat}$	Saturation factor	1,02

### 3.2 Simulation

First, the simulation of the stress analysis and deflection was performed for the 11.6 mm rotor disk thickness. The simulation itself included the entire rotor for the accuracy of the results since in many articles the analysis includes only a segment of the rotor.

The force between PMs on opposite rotor disks was applied on each magnet on the simulated rotor disk. Figures 7a and 7b show the Von Mises stress distribution on the rotor disk and the displacement for 11.6 mm rotor thickness, respectively. It is clear that the rotor thickness can be reduced from the mechanical point of view since the maximum deflection is only 0.0053 mm.

After a few simulations, it was determined that the 7 mm rotor thickness would be sufficient to withstand the forces between the adjacent PMs on opposite disks in such a way that the deflection remains acceptable.

Figures 8a and 8b show the Von Mises stress distribution on the rotor disk and the displacement of 7 mm rotor disk thickness, respectively. It can be seen from Figure 8a that the simulated deflection is 0.2171mm.

In [12], the author analysed the rotor disk thickness for this prototype AFPMM concerning the magnetic characteristics of the machine and determined that the characteristics are acceptable at 7 mm rotor thickness since there is practically no difference between magnetic flux density magnitudes calculated at 7 mm and 11.6 mm of rotor disk thickness. The simulation in Solidworks shows the same result for the mechanical point of view.

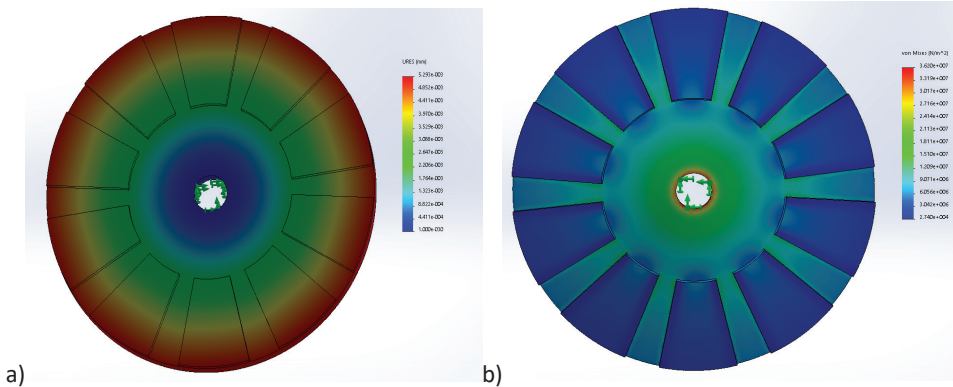


Figure 7: 11,6 mm rotor thickness: a) deflection, b) Von Mises stress distribution

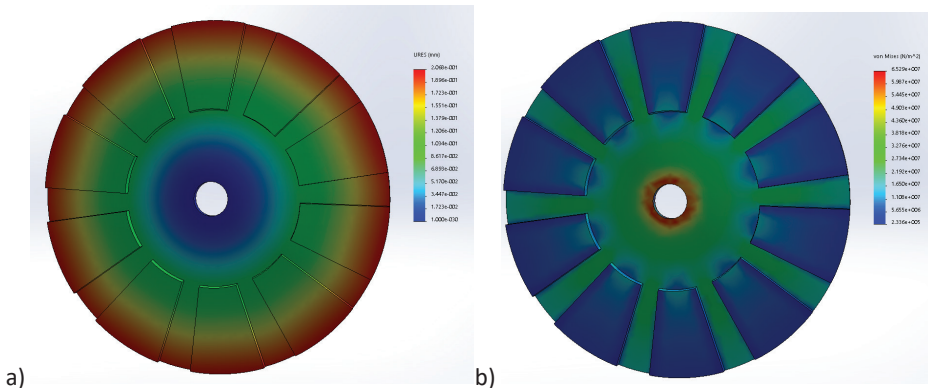


Figure 8: 7 mm rotor thickness: a) deflection, b) Von Mises stress distribution



### 3.3 Analytical verification

Equations for bending circular plates are derived in [15] and [16]. Timoshenko, [15], derived the differential equations for symmetrical bending of circular plates from observing the symmetrical distributed load acting on a circular plate.

In [16], the authors presented equations for various types of loads on a circular plate. Figure 10 shows the case that is suitable for a rotor disk of AFPMM with surface mounted PMs.

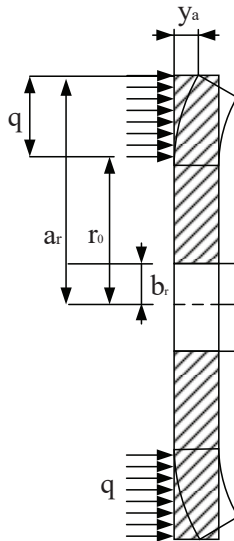


Figure 9: Circular plate bending

Equations for deflection calculations are:

$$y_a = M_{rb} \frac{a_r^2}{D} C_2 + Q_b \frac{a_r^3}{D} C_3 + q \frac{a_r^4}{D} L_{11} \tag{3.8}$$

$$M_{rb} = \frac{-qa_r^2}{C_8} \left( \frac{C_9}{2a_r b_r} (a_r^2 - r_0^2) - L_{17} \right) \tag{3.9}$$

$$Q_b = \frac{q}{2b_r} (a_r^2 - r_0^2) \tag{3.10}$$

$$C_2 = \frac{1}{4} \left( 1 - \left( \frac{b_r}{a_r} \right)^2 \left( 1 + 2 \ln \left( \frac{a_r}{b_r} \right) \right) \right) \tag{3.11}$$

$$C_3 = \frac{b_r}{4a_r} \left( \left( \left( \frac{b_r}{a_r} \right)^2 + 1 \right) \ln \left( \frac{a_r}{b_r} \right) + \left( \frac{b_r}{a_r} \right)^2 - 1 \right) \tag{3.12}$$

$$C_8 = \frac{1}{2} \left( 1 + \nu + (1 - \nu) \left( \frac{b_r}{a_r} \right)^2 \right) \tag{3.13}$$

$$C_9 = \frac{b_r}{a_r} \left( \frac{1 + \nu}{2} \ln \left( \frac{a_r}{b_r} \right) + \frac{1 - \nu}{4} \left( 1 - \left( \frac{b_r}{a_r} \right)^2 \right) \right) \tag{3.14}$$

$$L_{11} = \frac{1}{64} \left( 1 + 4 \left( \frac{r_0}{a_r} \right)^2 - 5 \left( \frac{r_0}{a_r} \right)^4 - 4 \left( \frac{r_0}{a_r} \right)^2 \left( 2 + \left( \frac{r_0}{a_r} \right)^2 \right) \ln \left( \frac{a_r}{r_0} \right) \right) \tag{3.15}$$

$$L_{17} = \frac{1}{4} \left( 1 - \frac{1 - \nu}{4} \left( 1 - \left( \frac{r_0}{a_r} \right)^4 \right) - \left( \frac{r_0}{a_r} \right)^2 \left( 1 + (1 + \nu) \ln \left( \frac{a_r}{r_0} \right) \right) \right) \tag{3.16}$$

$$D = \frac{Et^3}{12(1 - \nu^2)} \tag{3.17}$$

Table 4 presents the variables used in the set of equations (3.8)-(3.17) and their values.

Values of abovementioned variables are presented in Table 4 for a 7 mm rotor disk thickness.

**Table 4:** Variables used for deflection calculation

Symbol	Quantity	Value/Unit	
$y_a$	Deflection of rotor disks	0.20129 mm	
$M_{rb}$	Bending moment	469 Nm	
$a_r$	Outer radius of the disk	150 mm	
$b_r$	Inner radius of the disk	15 mm	
$r_0$	Radial location of unit line loading or start of a distributed load	80 mm	
$D$	Constant termed the "flexural stiffness" or "flexural rigidity",	6513 Pa mm <sup>3</sup>	
$Q_b$	Unit shear force (force per unit of circumferential length)	39979 Pa mm <sup>2</sup> /mm	
$q$	Magnetic pressure	74496 Pa	
$C_2, C_3, C_9$	Plate constants dependent upon the ratio $a=b$	$C_2$	0.2425
		$C_3$	0.0005
		$C_9$	0.0818
$L_{11}, L_{17}$	Loading constants dependent upon the ratio $a=r_0$	$L_{11}$	0.015994568091594
		$L_{17}$	0.112680595325043
$\nu$	Poisson's ratio	0,28	
$E$	Elastic module of the material used for rotor disks	210 GPa	
$t$	Thickness of the circular plate (rotor disk).	7 mm	

Using the equations described above, 0.20129 mm deflection was calculated for the 7 mm thick rotor disk. Magnetic pressure  $q$  was reduced by a factor that takes into account the area of magnets (multiplied by a coefficient  $\alpha_i$ ) since it is not constant over the area as marked on Figure 9.

Compared to the results obtained via the simulation, we can see that there is only 2.66% difference which is acceptable.

### 3 CONCLUSION

Using the Solidworks software and a set of analytical equations a new rotor disks thickness was determined for the analysed prototype AFPMM. MSA showed that, from a mechanical point of view, the existing rotor disks thickness can be reduced to 7 mm and maintain sufficient stiffness, so the air gap does not change significantly. By changing the thickness of the rotor disks, the weight of disks is reduced by approximately 40%.

### References

- [1] **Gieras JF, Wang RJ, Kamper MJ:** *Axial Flux Permanent Magnet Brushless Machines*, Springer Verlag, 2008
- [2] **W. Fei, P. C. K. Luk, and K. Jinupun:** *Design and analysis of high-speed coreless axial flux permanent magnet generator with circular magnets and coils*, *Electr. Power Appl. IET*, vol. 4, no. 9, pp. 739–747, 2010
- [3] **Xue, Y., Han, L., Li, H., Xie, L.:** *Optimal design and comparison of different PM synchronous generator systems for wind turbines*, *Int. Conf. Electrical Machines and Systems*, pp. 2448–2453, 2008
- [4] **Pinilla, M., Martinez, S.:** *Selection of main design variables for low-speed permanent magnet machines devoted to renewable energy conversion*, *IEEE Trans. Energy Convers.*, 26, (3), pp. 940–945, 2011
- [5] **M. Mirsalim, R. Yazdanpanah, and P. Hekmati:** *Design and analysis of double-sided slotless axial-flux permanent magnet machines with conventional and new stator core*, *IET Electr. Power Appl.*, vol. 9, no. 3, pp. 193–202, 2015
- [6] **H. Hatami, M. Bagher, B. Sharifian, and M. Sabahi:** *A New Design Method for Low-Speed Torus Type Afpm Machine for Hev Applications*, *IJRET*, Volume: 02 Issue: 12, pp. 396–406, 2013
- [7] **P. Vrtič, P. Pišek, T. Marčič, M. Hadžiselimović and B. Štumberger:** *Analytical Analysis of Magnetic Field and Back Electromotive Force Calculation of an Axial-Flux Permanent Magnet Synchronous Generator with Coreless Stator*, *IEEE Transactions on Magnetics*, vol. 44, no. 11, pp. 4333–4336, 2008
- [8] **P. Vrtič, M. Vražić, and G. Papa:** *Design of an axial flux permanent Magnet synchronous machine using analytical method and evolutionary optimization*, *IEEE Trans. Energy Convers.*, vol. 31, no. 1, pp. 150–158, 2016
- [9] **S. Kumar, T. A. Lipo, and B. Kwon:** *A 32,000 rev/min axial flux permanent magnet machine for energy storage with mechanical stress analysis*, *IEEE Trans. Magn.*, vol. 52, no. 7, pp. 1–1, 2016
- [10] **W. Fei, P. C. K. Luk, and T. S. El-Hasan:** *Rotor integrity design for a high-speed modular air-cored axial-flux permanent-magnet generator*, *IEEE Trans. Ind. Electron.*, vol. 58, no. 9, pp. 3848–3858, 2011

- [11] **J. A. Rani, E. Sulaiman, M. F. Omar, M. Z. Ahmad, and F. Khan:** *Computational Method of Rotor Stress Analysis for Various Flux Switching Machine Using J-MAG*, IEEE Student Conference on Research and Development (SCORED), 721–726, 2015
- [12] **P. Vrtič:** *Analysis of rotor disk thickness in coreless stator axial flux permanent magnet synchronous machine*, PRZEGLĄD ELEKTROTECHNICZNY, vol. ISSN 0033, no. 12, pp. 12–15, 2012
- [13] 2015 Solidworks Help Documentation
- [14] **M.A. Mueller, A.S. McDonald and D.E. Macpherson:** *Structural analysis of low-speed axial-flux permanent-magnet machines*, IEE Proceedings-Electric Power Appl., vol. 152, no. 6, pp. 1417–1426, 2005
- [15] **S. Timoshenko:** *Theory of Plates and Shells*, Second edition, 1987, McGraw-Hill Book Company, ISBN 0-07-064779-8
- [16] **W. C. Young and R. G. Budynas:** *Roark's Formulas for Stress and Strain*, vol. 7, no. 7th Edition. 2002
- [17] **P. Vrtič:** *Načrtovanje in analiza sinhronskih strojev s trajnimi magneti in aksialnim magnetnim pretokom*, Doctoral thesis, University of Maribor, 2009

## Nomenclature

(Symbols)	(Symbol meaning)
$R$	rotor disk radius
$d_{Fe}$	rotor disk thickness
$d_M$	permanent magnet thickness
$\tau_m$	magnetic pitch
$R_{iPM}$	inner radius of PM
$R_{oPM}$	outer radius of PM
$B_r$	remanent magnetic flux density
$\tau_p$	pole pitch
$p$	number of pole pairs
$I$	rated phase current
$A$	electrical current density
$P$	rated power at 1500 min <sup>-1</sup>
$N$	number of turns per coil
$d_c$	coil width

---

$d_s$	stator thickness
$\tau_c$	coil pitch
$m$	number of phases
$d_{ag}$	air-gap thickness
$S_w$	Copper wire cross section
$B_d$	airgap flux density
$\mu_0$	permeability of free space
$d_d$	fictitious air gap thickness
$k_{sat}$	saturation factor for iron
$\mu_r$	permeability of the steel
$\mu_{rec}$	relative recoil permeability
$S_{PM}$	active surface area of all PMs
$\alpha_i$	coefficient that is calculated with angle of PMs multiplied by the number of PMs per rotor disk (poles) and divided by 360 degrees
$q$	magnetic pressure
$F$	attractive force between adjacent magnets
$y_a$	deflection of rotor disks
$M_{rb}$	bending moment
$a_r$	outer radius of the disk
$b_r$	inner radius of the disk
$r_0$	radial location of unit line loading or start of a distributed load
$D$	stiffness factor of the material
$Q_b$	unit shear force (force per unit of circumferential length)
$C_2, C_3, C_9$	plate constants dependent upon the ratio $a=b$
$L_{11}, L_{17}$	loading constants dependent upon the ratio $a=r_0$
$\nu$	Poisson's ratio
$E$	elastic module of the material used,
$t$	thickness of the circular plate (rotor disk)